In-situ study of dislocation interaction with twin boundary and retraction in twinned metallic nanowires

Guangming Cheng[1,3*], Sheng Yin[2,4*], Chengjun Li[1], Tzu-Hsuan Chang[1], Gunther Richter[5], Huajian Gao[2,6,7#] and Yong Zhu[1#]

[1]Department of Mechanical and Aerospace Engineering, North Carolina State University, Raleigh, NC 27695, USA

[2]School of Engineering, Brown University, Providence, RI 02912, USA

[3]Princeton Institute for the Materials Science and Technology, Princeton University, Princeton, NJ 08540, USA

[4]Department of Materials Science and Engineering, University of California, Berkeley, CA 94720, USA

[5]Max Planck Institute for Intelligent Systems, Heisenbergstrasse 3, D-70589 Stuttgart, Germany

[6]School of Mechanical and Aerospace Engineering, College of Engineering, Nanyang Technological University, 70 Nanyang Drive, Singapore 639798, Singapore

[7]Institute of High Performance Computing, A*STAR, Singapore 138632, Singapore

[*]These authors contributed equally to this work.
#E-mail: huajian.gao@ntu.edu.sg; yong_zhu@ncsu.edu

Abstract

Metallic nanowires (NWs) with twin boundaries (TBs) running parallel to the NW length direction exhibit unusual plastic strain recovery owing to the interaction of dislocations with TBs. Here, based on *in-situ* transmission electron microscopy nanomechanical testing and molecular dynamics simulations, we report observation and quantification of dislocation nucleation, interaction with TBs, and retraction in bi-twinned Ag NWs **with a single TB along the NW length direction**. Our results show that leading partial dislocations nucleated from the free surface can be hindered by the TB, and upon unloading all or part of the leading partials can retract due to the repulsive force from the TB, leading to full or partial plastic strain recovery (Bauschinger effect), respectively. The bi-twinned Ag NWs can undergo stress relaxation, even at a stress below the yield strength, where the plastic strain also recovers upon unloading. Our results illustrate that the internal TBs in NWs can interact with surface-nucleated dislocations, leading to time-dependent plastic strain recovery and Bauschinger effect.

Keywords: Dislocation slip, Twin boundary, Recoverable plasticity, Nanomechanical test, MD simulations, *in-situ* TEM

1. Introduction

Metallic nanowires (NWs) are important building blocks for a wide range of applications, including transparent electrodes and flexible and stretchable electronics [1, 2], due to their high electric conductivity and optical transmittance. In addition, metallic NWs usually exhibit ultrahigh mechanical strength and are ideal candidates for studying fundamental deformation mechanisms at the nanoscale [3-12]. More specifically, dislocation nucleation from free surfaces has become dominant, in contrast to the forest dislocation dynamics in bulk materials.[13-22] The deformation mechanisms in face-centered cubic (FCC) single crystalline metallic NWs have been extensively studied.[23-25] Competing mechanisms including slip by partial dislocations, slip by full dislocations, and twinning have been reported [7, 11, 26], which can be understood based on the Schmid factors for the leading and trailing partials and the generalized stacking fault energies. Recently, we have found that an additional factor, cross-sectional shape, can also affect the competition between the deformation mechanisms.[9, 10]

It is common to introduce twin boundaries (TBs) in NWs during the synthesis.[27, 28] Metallic NWs with internal TBs have received much attention recently, such as metallic NWs with parallel, inclined or perpendicular TBs with respect to the NW length direction [6, 29-36]. In particular, NWs with multiple TBs parallel to the NW length direction have been reported to exhibit unusual time-dependent mechanical behavior. For example, a type of recoverable plasticity was observed in penta-twinned Ag NWs with five TBs running parallel to the NW length direction [27, 28]. However, due to the overlap of five twin variants in a penta-twinned NW, it was not possible to directly observe dislocation interactions with the TBs.

Interaction between dislocations and TBs has become one of the most fundamental problems in materials science due to the emergence of nanotwinned materials over the past 2 decades.[37-43] TBs have been shown able to simultaneously enhance the strength, ductility and fracture toughness of nanotwinned metals [40, 44, 45], ceramics [46-48] and biomaterials [49], in which dislocation-TB interactions [37, 39, 50] plays a crucial role. In general, NWs have been used to probe several deformation mechanisms, such as the effect of surface diffusion on dislocation nucleation [7, 51, 52], hydrogen embrittlement [21, 53], and brittle-to-ductile transition [13, 54, 55], to name a few. The twinned metallic NWs can provide an interesting platform to investigate the energetics and kinetics of dislocation-twin boundary interactions.

Here, we report real-time observation of dislocation nucleation, interaction with the TBs and retraction, while simultaneously measuring the stress and strain in bi-twinned Ag NWs (with a single TB running parallel to the NW length direction) via quantitative *in-situ* transmission electron microscopy (TEM) tensile tests, using a state-of-the-art microelectromechanical system (MEMS) stage. *In situ* TEM tests and molecular dynamics (MD) simulations show that leading partial dislocations nucleated from the free surface can be hindered by the single TB in the bi-twinned Ag NWs, while they can be retracted due to the repulsive force from the single TB, leading to plastic strain recovery. Additional *in situ* tensile testing shows that stress relaxation can occur in bi-twinned Ag NWs at an applied stress below the yield strength.

2. Methods

2.1 Sample synthesis and characterization

Crystalline Ag NWs were synthesized by physical vapour deposition inside a molecular beam epitaxy system under ultra-high vacuum condition and substrate temperature of 700 °C. Penta-twinned Ag NWs were synthesized by reducing $AgNO_3$ with ethylene glycol in the presence of polyvinyl pyrrolidone. The solution of Ag NWs was diluted with deionized water and then purified by centrifugation. More details of the NW synthesis process are provided elsewhere .[56]

Cross-sectional TEM samples of Ag NWs after deformation were prepared with focused ion beam (FIB). High-resolution TEM observations were performed on JEOL 2010F with a Schottky field emission gun (FEG) operated at 200 kV. Atomic resolution high-angle annular dark-field (HAADF) scanning transmission electron microscopy (STEM) imaging was performed on a probe corrected FEI Titan G^2 80-300 kV S/TEM equipped with an X-FEG source operated at 200 kV.

2.2 *In situ* SEM/TEM mechanical testing

Mechanical testing was carried out *in situ* inside a TEM using a MEMS-based material testing system, which consists of an electrostatic (comb-drive) actuator, a capacitive load sensor and a gap in between for mounting samples (Fig. 1a). Details on the load sensor calibration have been reported previously.[54, 57] Displacement (and strain) is measured by digital image correlation of TEM images of two fiducial markers on the specimen (Fig. 1b). This MEMS-based system has a strain resolution of 0.01% (gage length 2 μm) and a stress resolution of 1.4 MPa (for example, for NW diameter of 104 nm [28]).

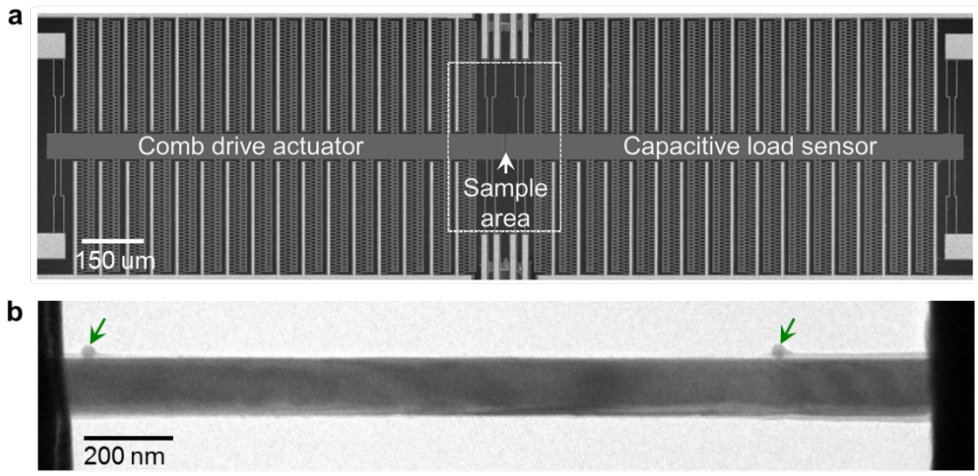

Fig.1. *In situ* TEM tensile testing system. (a) Comb-drive-actuated MEMS device for tensile test. (b) TEM image showing a NW mounted on the device. Two fiducial markers are deposited on the NW surface for displacement (or strain) measurement.

NWs were mounted on the testing stage using a nanomanipulator (Klocke Nanotechnik, Germany) inside a FEI Nova 600 dual beam. An Ag NW was welded to the nanomanipulator probe, then mounted to the MEMS stage and clamped by electron-beam-induced Pt deposition at the two free ends. Two fiducial markers were deposited on the NWs for displacement (and strain) measurement. *In situ* TEM mechanical testing was performed on JEOL 2010F operated at 200 kV. The loading and unloading strain rates were ~0.003%/s. Low magnification images were recorded at a fixed condense (the second condense lens) current to minimize the focus change. The current density of incident e-beam is < 0.1 A/cm^2 [58] and its effect on the mechanical behavior of the NW under tensile testing can be neglected.

2.3 MD simulations

Large-scale MD simulations were performed using the software package LAMMPS [59]. Bi-twinned NW sample was generated according to experimentally observed shapes. Figure 7 shows the atomic cross-section of the bi-twinned NW sample which is about 15 nm in both height and width and 50 nm in length. The embedded atom method potential for Ag is used to describe the interatomic interactions [60]. The samples are initially relaxed and equilibrated at temperature of 300 K for 600 ps using the Nosé–Hoover thermostat and barostat. Periodic boundary condition is imposed along the axial direction (that is, the loading direction <110>). During loading, the samples are stretched at a constant strain rate of $10^8\,s^{-1}$ under NVT ensemble (canonical ensemble). During relaxation, the strain of the sample is fixed and NW is relaxed under NVT ensemble for 2 nanoseconds. During the relaxation step, we monitor the variation of the axial stress by averaging the virial stresses over all atoms in the samples. To examine the reversibility of deformation (related to the reverse motion of dislocations), we unload the elongated samples at a strain rate of $-10^8\,s^{-1}$.

3. Results

3.1 Characterization of bi-twinned NWs

Crystalline Ag NWs were synthesized by physical vapour deposition inside a molecular beam epitaxy system [4]. A scanning electron microscope (SEM) image in Fig. 2a shows Ag NWs on Si substrate, with length of 5-25 um and width of 50-200 nm. The width distribution of Ag NWs, measured directly from TEM image of 132 NWs, is shown in Fig. 2b. Based on the TEM characterization, two types of <110> oriented Ag NWs were identified in the synthesized product, one being bi-twinned and the other single crystalline

NWs. Bi-twinned NWs exhibit a single internal TB running parallel to the NW length direction as shown in Fig. 2c, which count 81.8% of the 132 examined NWs (Fig. 2b).

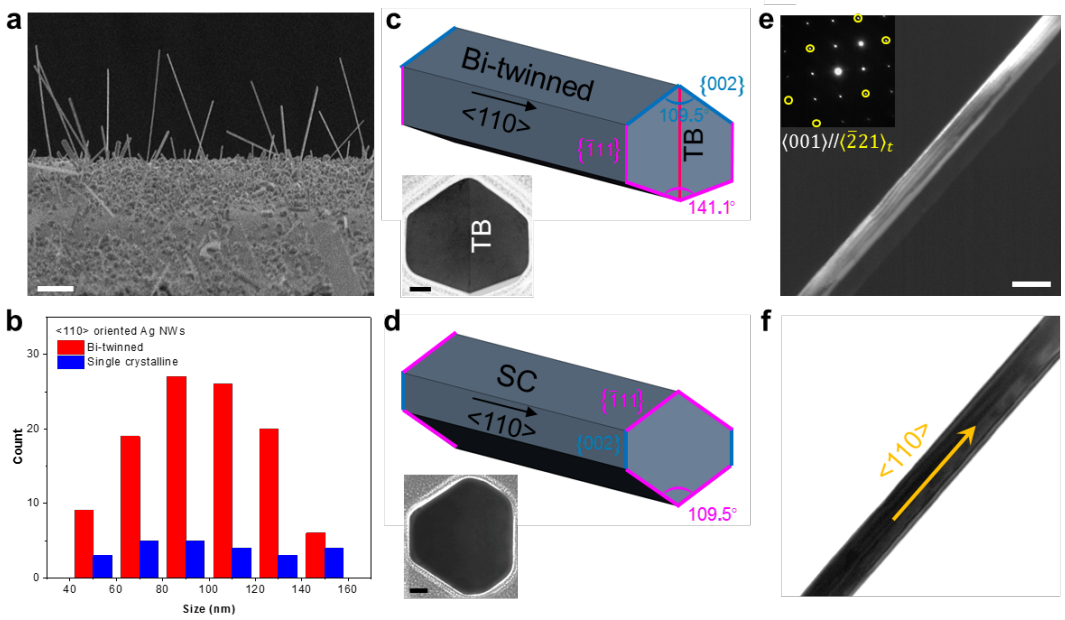

Fig. 2. (a) SEM image of Ag NWs on Si substrate. (b) Size distribution of Ag NWs (132 NWs examined). (c,d) Schematic drawings of bi-twinned and single crystalline NWs and corresponding cross-sectional TEM images. Scale bar, 20 nm. (e,f) Dark- and bright-field TEM images of a bi-twinned NW from the longitudinal view. Inset in (e) is the corresponding composite diffraction pattern taken from <001> and <$\bar{2}$21>$_t$ zone axes. The sub-t represents the twin variant. Scale bar, 100 nm.

In experiments, the type of Ag NWs can be directly determined from cross-sectional TEM images, shown in the insets in Fig. 2c,d. Both bi-twinned and single crystalline NWs exhibit hexagonal cross-sectional shapes but different arrangement of surface facets (marked in Fig. 2c,d). A bi-twinned NW shows clearly a TB between two twin variants

(see the inset in Fig. 2c). Based on the geometry of the bi-twinned structure (see Fig. 2c and 3), there is a 19.4° tilt angle between $\langle 1\bar{1}0 \rangle$ and $<001>_t$ zone axes from the two twin variants, which can be used as a criterion for determining bi-twinned NWs under the longitudinal view since there is a 45° or 90° included angle between $\langle 1\bar{1}0 \rangle$ and <001> in single crystalline NWs. The bi-twinned structure can be distinguished by comparing the dark- and bright-field TEM images when viewed from the zone axes of $\langle 1\bar{1}0 \rangle$ or <001> from one of the twin variants. Fig. 2e,f shows an example of a bi-twinned Ag NW viewed from the <001> and $<\bar{2}21>_t$ zone axes of the twin variants (see the composite diffraction pattern in the inset of Fig. 2e and 3b). The twin variant from <001> zone axis showed bright image contrast under dark-field TEM imaging mode (Fig. 2e), although the two twin variants displayed weak image contrast under bright-field imaging mode (Fig. 2f).

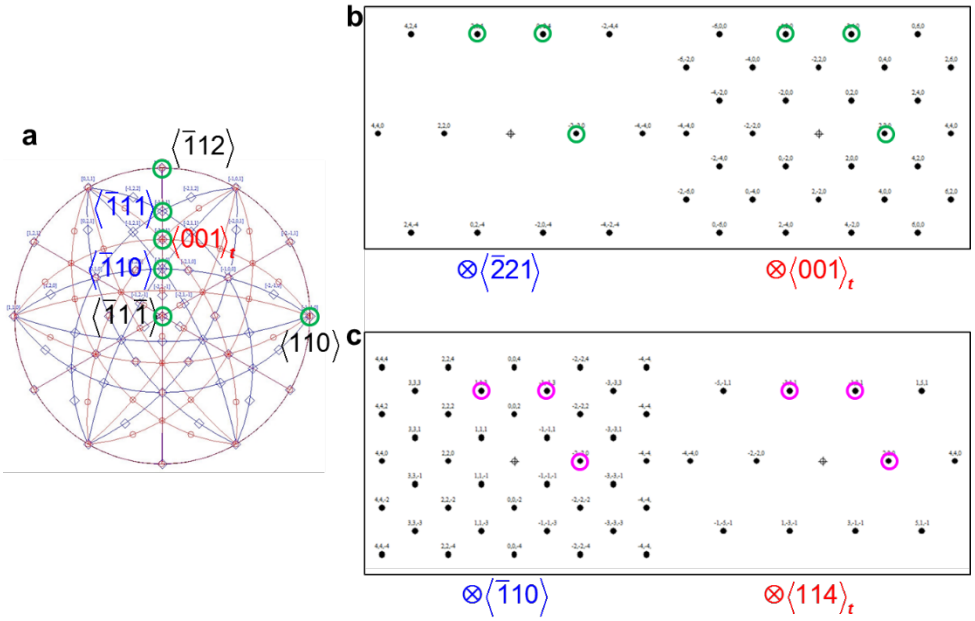

Fig. 3. Characterization of the bi-twinned structure. (a) A composite kikuchi pattern for the two twin variants in bi-twinned NWs. Blue and red indices are from the two variants, respectively. Black indices are from the same indices of the two variants. The tilt angle

between <110> and <001>t is 19.4°, which can be used as a criterion for determining the bi-twinned structures. (b) Simulated diffraction patterns of the two twin variants at on-zone condition in which one of them is at zone axes of <110> or <001>. The spots marked by circles represent the positions where the high-index diffraction pattern is fully overlapped with the low-index diffraction pattern.

3.2 *In situ* observation of dislocation nucleation and retraction

We performed *in-situ* TEM tensile testing of individual NWs using a MEMS-based testing stage (see Fig. 1) that allows accurate measurement of both load and displacement [61-63]. Figure 4 shows the stress-strain responses and snapshots of microstructure evolution during typical loading-unloading cycles of a bi-twinned Ag NW with or without a holding step. Note that the viewing direction in Fig. 4c,d is from the $\langle 1\bar{1}0 \rangle$ zone axis as marked by the orange arrow in the inset in Fig. 4a. Figure 4a,c shows a loading-unloading cycle without the holding step (Movie 1). As a partial dislocation (marked by A in Fig. 4c-ii) came out during loading (with the applied stress, 1.46GPa, slightly over the yield strength, 1.41GPa, see Fig. 5), we immediately started unloading the NW by decreasing the applied force. It was observed that another partial (marked by B in Fig. 4c-iii) appeared at the initial stage of unloading. As the applied stress continued to decline, the later generated partial B first disappeared (Fig. 4c-iv) when the applied stress was decreased by 75%. Subsequently, partial A also disappeared as the applied loading was fully released. At this point, the plastic strain was almost recovered after fully releasing the applied force. This suggests that, in the absence of an applied stress, the TB provides a repulsive force for the leading partials to retract and disappear.

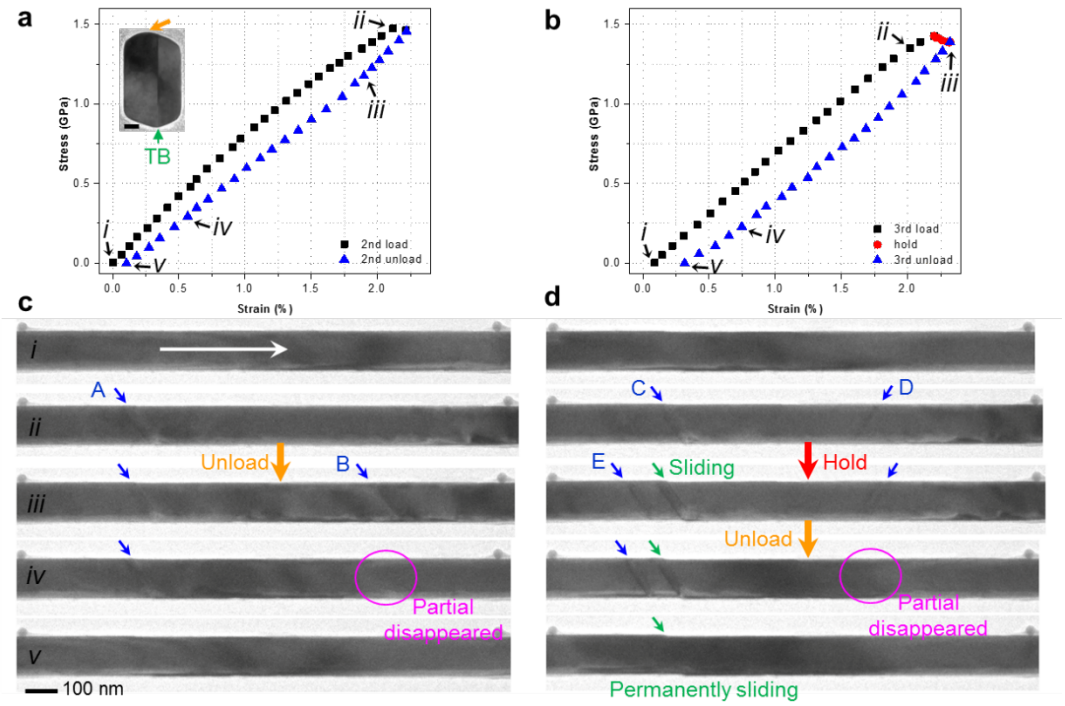

Fig. 4. Mechanical responses and microstructure evolution of a bi-twinned Ag NW under *in-situ* TEM tensile testing. (a,b) Stress-strain curves for the bi-twinned NW without or with a holding step, respectively. The relaxation step took 5 minutes. Inset in (a) is the corresponding cross-sectional images of the tested NW (sectioned from the undeformed part after the test). Location of the TB is marked by a green arrow. Scale bar, 20 nm. (c,d) Snapshots of microstructure evolution during loading-unloading and loading-holding-unloading processes, respectively. The location of partial dislocations and planar slip in the NW are marked by blue and green arrows, respectively. Scale bar, 100 nm. The viewing direction in (c,d) is from the $\langle 1\bar{1}0 \rangle$ zone axis as marked by the orange arrow in the inset in (a).

Figure 4b,d displays a loading-unloading cycle with a short-time (5 minutes) stress relaxation under a fixed applied load (Movie 2). Two partials (marked by C and D in Fig. 4d-ii) came out as the applied stress went over the yield strength. During the holding step, a new partial (marked by E in Fig. 4d-iii) was generated and an obvious planar sliding was observed (located at C). The planar sliding was due to the propagation of dislocations across the entire cross-section. During the unloading step, partial D first disappeared as the applied stress was decreased by 80% (Fig. 4d-iv) and partial E disappeared when the applied stress was totally released, but there was a step permanently left at position C (Fig. 4d-v). Note that there is residual strain (~0.2%) left in the NW due to the permanent planar sliding (position C) which cannot be fully recovered after holding 15 minutes at zero stress. Accordingly, the above results suggest that the internal TB in the bi-twinned NWs can act as an obstacle for hindering the propagation of partial dislocations across the TB in the time when the applied stress is slightly over the yield strength and facilitate retraction of the partials upon unloading.

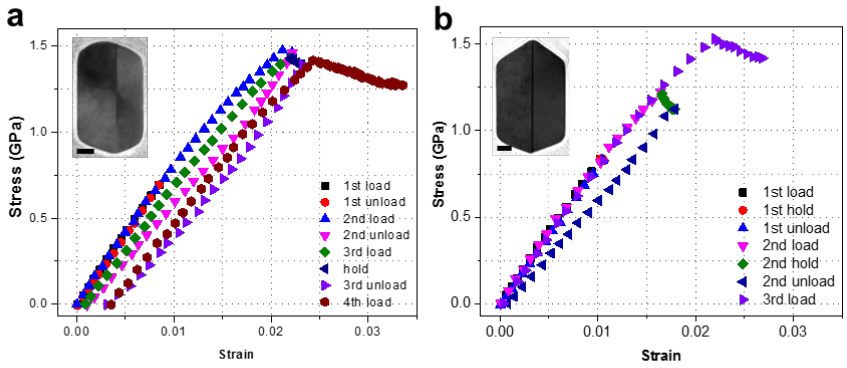

Fig. 5. Stress-strain curves for the tested bi-twinned NWs in Figs. 3 and 6, respectively. Insets in (a) and (b) show the cross-sectional TEM images of the tested NWs. All scale bars, 20 nm.

3.3 Stress relaxation in bi-twinned NWs

The above *in-situ* TEM observations confirmed that partial dislocations hindered by the single TB in a bi-twinned NW can be retracted during unloading under the repulsive force from the TB. Note that we started unloading or holding steps in the above experiments once we observed the first event of dislocation nucleation in the NWs. In this sense, the applied stress was over the yield strength. However, stress relaxation can occur at an applied stress below the yield strength as reported in the penta-twinned NWs with multiple TBs [28]. In order to corroborate if the stress relaxation can occur in bi-twinned NWs, we did additional *in-situ* relaxation experiments by applying the stress lower than the yield strength.

Figure 6a shows the stress-strain responses during typical tensile tests (two cycles) of a bi-twinned Ag NW in three steps: loading, relaxation and unloading. Two levels of applied stresses were chosen for stress relaxation (held about 15 minutes with a fixed applied force). One (1.21GPa) is close to the yield strength (1.37GPa, see Fig. 5a), while the other (0.84GPa) is substantially lower than the yield strength. During the loading step, the NW in both cases exhibited nearly linear response. During the relaxation step, there was an obvious change of stress and strain with time (the stress decreased while the strain increased) at the larger applied stress, while almost no relaxation took place at the smaller applied stress. On unloading, the strain in the NW completely recovered for both cases. Figure 6b shows the detailed behaviors of strain and stress as functions of time at the two selected stress levels during the stress relaxation step. For the larger applied stress, the NW strain increased monotonically with time from 1.66 to 1.79%, while the stress decreased monotonically from 1.21 to 1.12GPa. However, for the smaller applied stress (0.84GPa),

there was no obvious change of strain and stress during the relaxation step. This is different from the phenomenon observed in penta-twinned Ag NWs shown in Fig. 6c,d [28] that stress relaxation can even take place at a very small initial stress (0.37GPa), which is far below the yield strength (1.0GPa). Detailed comparison of the mechanism in the two types of twinned NWs will be discussed later.

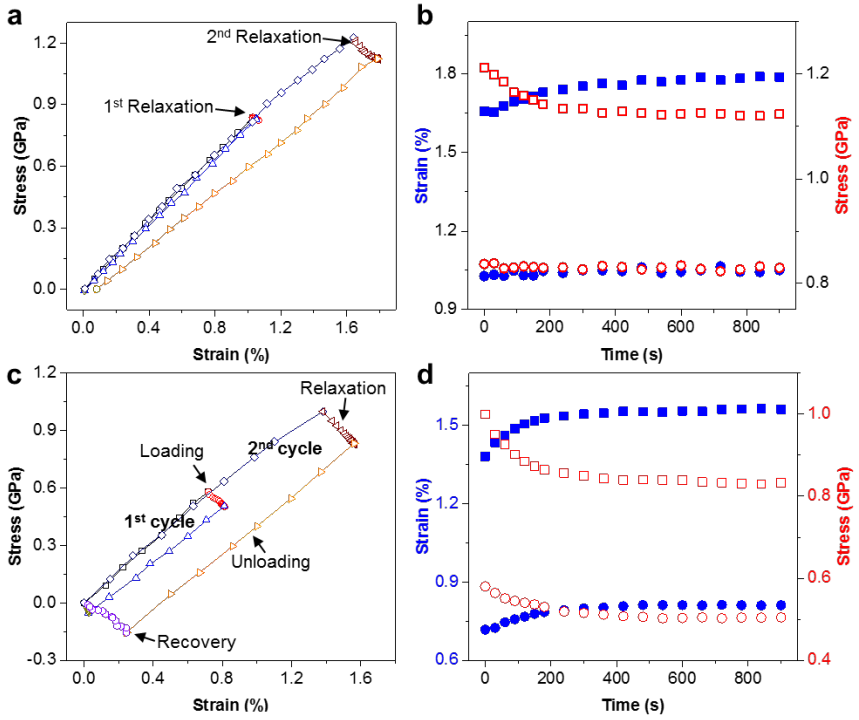

Fig. 6. *In-situ* measurements of stress and strain evolutions in bi- (a,b) and penta-twinned (c,d) Ag NWs [28]. (a,c) Stress-strain curves for the bi- and penta-twinned NWs under two cycles of loading-relaxation-unloading-recovery, respectively. The relaxation and recovery steps took 15 minutes. (b,d) Relaxation curves for the bi- and penta-twinned NWs, respectively. Solid and open symbols correspond to the strain-time and stress-time relationships, respectively. Square and circle symbols correspond to high and low initial stress levels, respectively.

3.4 MD simulations of dislocation nucleation and retraction

MD simulations were performed to further understand the underlying mechanisms behind the observed relaxation and recovery behaviors in bi-twinned NWs. Figure 7 shows the simulated results from a bi-twinned Ag NW underwent loading-unloading cycles with or without a relaxation step, in accordance with the *in-situ* experiments in Fig. 3. Figure 7a shows the stress-strain curve without a relaxation step. Similar to the case in Fig. 3a, the NW was unloaded as soon as partial dislocations came out during the loading step. After yielding, leading partials were generated from the NW surface, glided in the NW, and blocked by the TB. Initially, three partials were nucleated and all blocked by the TB (Fig. 7b). When the external stress decreases during unloading, a repulsive force from the TB [64] can induce a reverse motion of dislocations by pushing their non-inserted segments as well as extracting their inserted segments from the TB. Thus, during unloading, these partials can gradually retract from the TB (Fig. 7b(i-iii)); the corresponding part of the plastic strain is recoverable (Fig. 7a). In this case, all the nucleated partials were blocked by the TB and finally retracted from the TB, resulting in a complete plastic strain recovery (Fig. 7a).

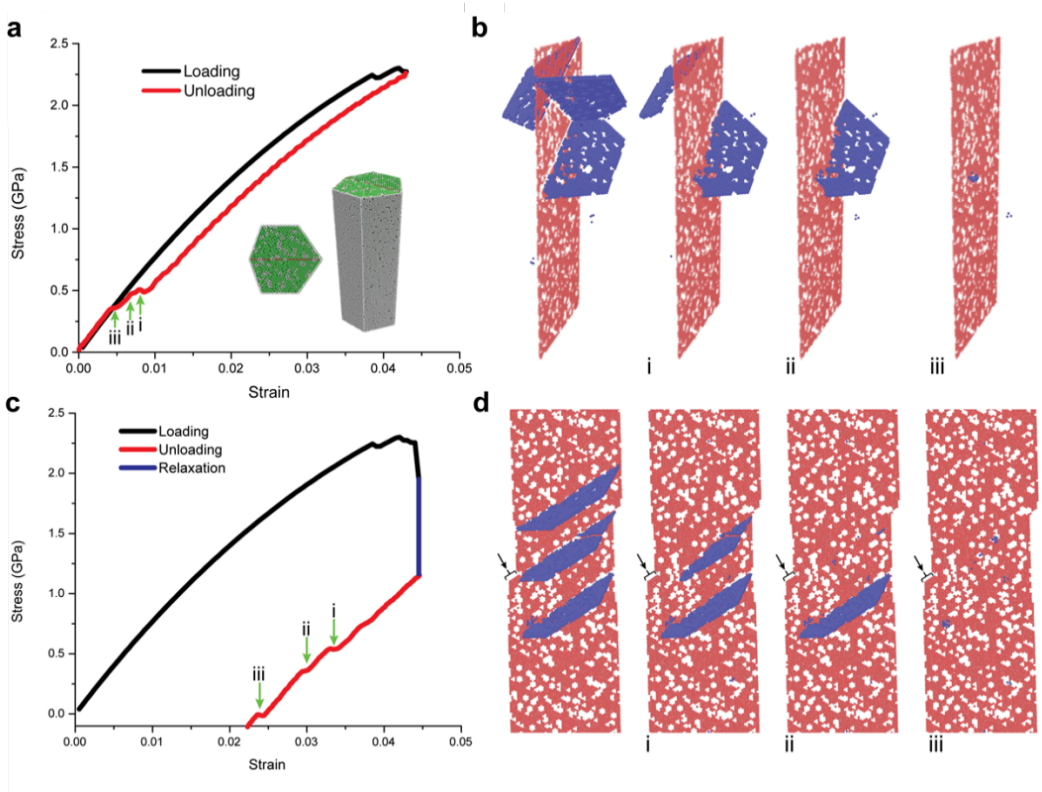

Fig. 7. MD simulations of stress relaxation and strain recovery in a bi-twinned Ag NW. (a) Stress-strain curve of the loading-unloading process. Insets in (a) is the atomic models. (b) Snapshots of partial dislocation retraction during unloading (only HCP atoms are shown, with TB colored in red and stacking faults colored in blue). (c) Stress-strain curve of the full loading-relaxation-unloading process. (d) Snapshots of partial dislocation retraction during unloading. The black arrow indicates a permanent slip step created by full dislocation gliding. The green arrows i,ii,iii during unloading in (a,c) correspond to the retraction event of three partials blocked by the TB.

Also simulated is the loading-unloading behavior with a relaxation step in between (Fig. 7c). First the NW was stretched to a strain of 4.45% over the yielding point, and then stress relaxation was monitored while the applied strain was fixed. After stress relaxation, the

simulated sample was subsequently unloaded. In this simulation, after yielding, several leading partials were generated from the NW surface, glided in the NW, and blocked by the TB. During relaxation, some of the leading partials transmitted across the TB, after which trailing partials were generated from the NW surface and followed the leading partials to form full dislocations, leaving behind a permanent surface step (pointed out by the black arrow in Fig. 7d) in the region where the leading and trailing partials keep sweeping through the cross-section and the stress gradually decreased from an initial value of 1.81GPa by about 630MPa. The continuous nucleation of partial dislocations during the stress relaxation step indicates that the stress relaxation is a direct consequence of dislocation nucleation in bi-twinned NWs. After the relaxation, besides the permanent slip, several leading partials were still blocked by the TB and left the stacking faults in one of the grains in the bi-twinned NW (Fig. 7d). Similar to the step in Fig. 7b during unloading, these partials blocked by the TB can also gradually retract (Fig. 7d(i-iii)) and the corresponding part of plastic strain is recoverable (Fig. 7c); the region marked by the black arrow in Fig. 7d (a surface step) is not recoverable, as well as the corresponding part of plastic strain in Fig. 7c. This is consistent with the experimental results in Fig. 3, in which full recovery can occur only if all partials are blocked by the TB. Once permanent sliding occurs, only partial plastic strain recovery can occur. Such a phenomenon can be related to the classic Bauschinger effect of partial plastic recovery during unloading. We can see asymmetric plastic flow, and partial or full recovery of plastic deformation upon unloading in Figs. 3 and 7. However, this effect in bi-twinned NWs is much weaker compared to penta-twinned NWs [27], which will be discussed later.

In brief, recoverable plasticity in bi-twinned NWs has been observed and correlated with the nucleation and retraction of partial dislocations which are blocked by an internal TB in such NWs. Nucleation of partial dislocations from the free surface mainly contributed to the stress relaxation on loading, and retraction of partial dislocations contributed to the plastic strain recovery on unloading. The internal TB in bi-twinned NWs acts as an obstacle for hindering the propagation of some partial dislocations, making the corresponding part of plastic strain recoverable. In cases dislocations directly traveled through the entire cross-section of bi-twinned NWs or twinning occurred in single crystalline NWs, permanent plastic deformation would occur.

4. Discussions

As we know, the internal TBs in bi-twinned NWs play an important role in the observed recoverable plasticity owing to the nucleation and retraction of partial dislocations. For comparison, Fig. 8 shows the stress-strain response and snapshots of microstructure evolution during a typical tensile test of a single crystalline Ag NW (Movie 3). The loading direction was along the NW length direction and there was no extended defect in the NW prior to loading (Fig. 8b-i). As the applied stress reached the yield strength (1.0 GPa), a planar sliding (marked in Fig. 8b-ii) quickly occurred in the NW and the strain was obviously increased. During the unloading step, a small deformed segment was left in the NW (Fig. 8b-iii and iv) and the NW showed only elastic unloading (i.e., linear strain-stress behavior). This indicates that the planar sliding formed during loading was a permanent plastic deformation. Therefore, there is no recoverable plasticity in single crystalline NWs. It should be mentioned that recoverable plasticity in twinned NWs with inclined or

perpendicular TBs to the NW length direction is insignificant because dislocations nucleated from the free surface are prone to travelling through the entire cross section, leading to permanent plastic deformation [33].

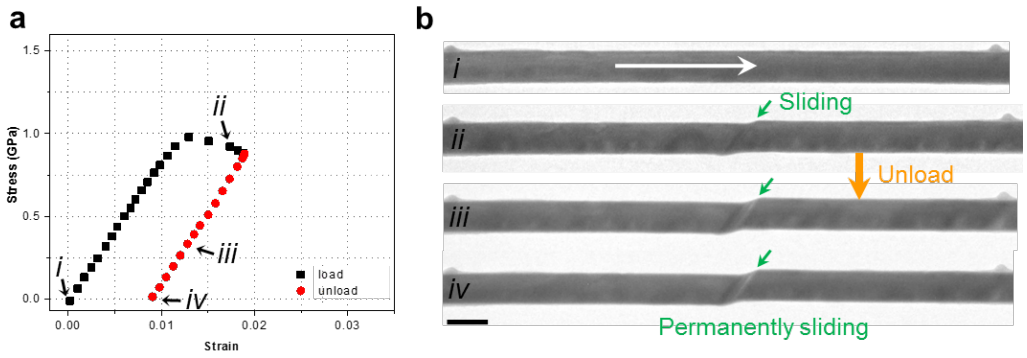

Fig. 8. (a) Stress-strain curve for a single crystalline Ag NW under *in-situ* TEM tensile testing. (b) Snapshots of microstructure evolution during the loading-unloading process. Permanent planar sliding in the NW is marked by the green arrows. Scale bar, 100 nm.

Although recoverable plasticity is observed in both bi- and penta-twinned NWs [28] with TBs parallel to the NW length direction, there exist significant differences between them, including the stress relaxation, strain recovery, and the interaction between dislocations and TBs, which can be attributed to difference in their microstructures. Stress relaxation in bi-twinned NWs requires a higher stress level than that in penta-twinned NWs. It has been shown that pre-existing defects in penta-twinned NWs can promote the nucleation of partial dislocations (i.e. lower the stress threshold for dislocation nucleation) [28]. However, bi-twinned NWs in this study exhibit high crystalline quality with nearly no pre-existing defects in the twin variants (Fig. 2 and 9a). In this system, partial dislocations can only nucleate from the free surface, and glide into the grain interior. Thus, a higher yield stress is required for the nucleation of partial dislocations in bi-twinned NWs. On the other

hand, plastic strain recovery in bi-twinned NWs is almost complete during the unloading step, while an additional strain recovery step is needed for penta-twinned NWs. It appears that penta-twinned NWs only show elastic strain recovery during the unloading step and reach full plastic strain recovery during the additional recovery step [28]. The delay of the plastic strain recovery in penta-twinned NWs could be attributed to the impediment of pre-existing defects on the retracting dislocations (Fig. 9b). In contrast, in bi-twinned NWs, due to their high crystalline quality, the blocked partials could retract without impediments, leading to a speedy recovery of the plastic strain. Another notable difference is that, in penta-twinned NWs, the dislocation motion is influenced by the inhomogeneous stress field generated by the fivefold twin structure that can be regarded as a disclination with an angular deficiency of 7.35º. Obviously, such an inhomogeneous strain field does not exist in bi-twinned NWs.

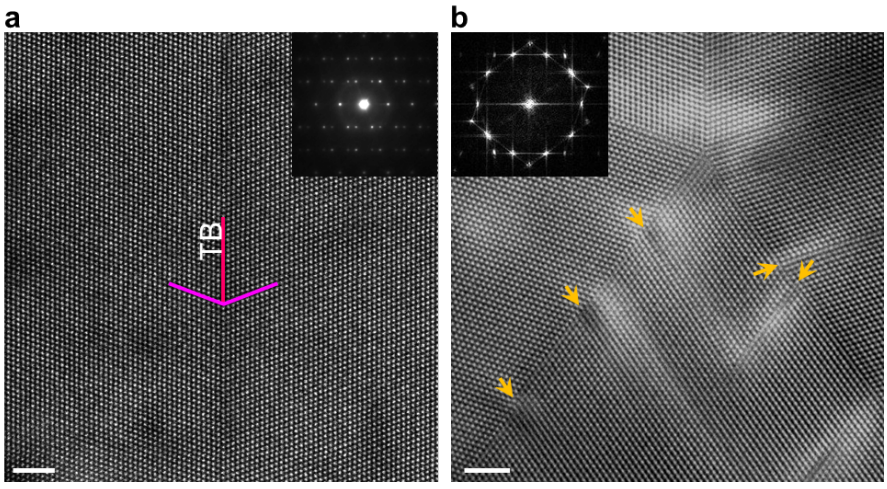

Fig. 9. HAADF-STEM images showing the atomic alignment along the TB from the cross-sectional view of bi-twinned (a) and penta-twinned (b) Ag NWs. The inset in (a,b) is the corresponding SAED pattern. Scale bar, 2 nm.

In addition to full plastic strain recovery, interaction between partial dislocations and TBs can result in Bauschinger effect in both bi- and penta-twinned NWs. However, penta-twinned NWs exhibit much stronger Bauschinger effect than bi-twinned NWs, which is manifested in two ways – showing larger recovered plastic strain for each unloading and sustaining more loading/unloading cycles up to larger failure strain. This is related to the microstructures and dislocation mechanisms in bi- and penta-twinned NWs. In bi-twinned NWs, a leading partial can transmit across the single TB relatively easily, considering their larger yield strength than penta-twinned NWs. A trailing partial may follow sweeping across the entire cross section and gliding out of the NW at the opposite surface, leading to a permanent planar slip step [9]. Bi-twinned NWs can store much fewer retractable dislocations and typically fail at smaller strain than penta-twinned NWs. In penta-twinned NWs, a leading partial in one twin variant can trigger dislocation activity in neighboring twin variants, leading to the formation of stacking fault decahedrons (SFDs) [27, 28]. Unlike the permanent slip via full dislocation escaping in bi-twinned NW, SFDs are fully reversible, but further dislocation reactions and entanglements can lead to only partial plastic recovery. Penta-twinned NWs exhibit relatively strong strain hardening and tensile ductility as a result of the effective obstruction of surface-nucleated dislocations by TBs [36]. The strain hardening in turn is responsible for the pronounced Bauschinger effect under cyclic loading. Similar phenomena have also been reported in heterostructured metals [65-68], which was attributed to the high back stress associated with interactions between dislocations and grain or twin boundaries.

5. Conclusions

In summary, in-situ TEM observations showed that leading partial dislocations nucleated from the free surface of a bi-twinned Ag NW can be obstructed by the single TB, and that the blocked partials can be retracted under the repulsive force from the TB during unloading, leading to plastic strain recovery or Bauschinger effect. Some leading partials can transmit across the TB followed by trailing partials, leading to permanent slip and partial plastic strain recovery. Additional *in-situ* experiments showed that bi-twinned Ag NWs can undergo stress relaxation on loading at an applied stress below the yield strength. This confirmed that the internal TB in bi-twinned NWs can act as an obstacle for hindering the propagation of partial dislocations across the TB. Significant differences were found in the observed recoverable plasticity in bi- and penta-twinned [28] Ag NWs, including stress relaxation, strain recovery, and interaction between dislocations and TBs, due to differences in their microstructure configurations and dislocation mechanisms. The observed full and partial recoverable plasticity in twinned NWs provides important new insights into the understanding of interactions between dislocations and TBs in twinned metallic nanomaterials.

Acknowledgements

G.C. and Y.Z. acknowledge financial support from the National Science Foundation (NSF) under Award Nos. CMMI-1762511 and 1929646. S.Y. and H.G. acknowledge financial support from the NSF through Grant DMR-1709318 and computational support by the Extreme Science and Engineering Discovery Environment (XSEDE) through Grant MS090046. The authors acknowledge the use of the Analytical Instrumentation Facility (AIF) at North Carolina State University, which is supported by the State of North Carolina

and the National Science Foundation (award number ECCS-1542015). The AIF is a member of the North Carolina Research Triangle Nanotechnology Network (RTNN), a site in the National Nanotechnology Coordinated Infrastructure (NNCI).

References

[1] J.-Y. Lee, S.T. Connor, Y. Cui, P. Peumans, Solution-processed metal nanowire mesh transparent electrodes, Nano letters 8 (2008) 689-692.
[2] F. Xu, Y. Zhu, Highly conductive and stretchable silver nanowire conductors, Advanced materials 24 (2012) 5117-5122.
[3] B. Wu, A. Heidelberg, J.J. Boland, Mechanical properties of ultrahigh-strength gold nanowires, Nature Materials 4 (2005) 525-529.
[4] G. Richter, K. Hillerich, D.S. Gianola, R. Moenig, O. Kraft, C.A. Volkert, Ultrahigh Strength Single Crystalline Nanowhiskers Grown by Physical Vapor Deposition, Nano Letters 9 (2009) 3048-3052.
[5] T. Zhu, J. Li, Ultra-strength materials, Progress in Materials Science 55 (2010) 710-757.
[6] J. Wang, F. Sansoz, J. Huang, Y. Liu, S. Sun, Z. Zhang, S.X. Mao, Near-ideal theoretical strength in gold nanowires containing angstrom scale twins, Nature communications 4 (2013) 1742.
[7] L.Y. Chen, M.-r. He, J. Shin, G. Richter, D.S. Gianola, Measuring surface dislocation nucleation in defect-scarce nanostructures, Nature Materials 14 (2015) 707-713.
[8] S. Lee, J. Im, Y. Yoo, E. Bitzek, D. Kiener, G. Richter, B. Kim, S.H. Oh, Reversible cyclic deformation mechanism of gold nanowires by twinning–detwinning transition evidenced from in situ TEM, Nature communications 5 (2014) 3033.
[9] G. Cheng, S. Yin, T.H. Chang, G. Richter, H. Gao, Y. Zhu, Anomalous Tensile Detwinning in Twinned Nanowires, Physical Review Letters 119 (2017) 256101.
[10] S. Yin, G. Cheng, Y. Zhu, H. Gao, Competition between shear localization and tensile detwinning in twinned nanowires, Physical Review Materials 4 (2020) 023603.
[11] S. Yin, G. Cheng, G. Richter, H. Gao, Y. Zhu, Transition of Deformation Mechanisms in Single-Crystalline Metallic Nanowires, Acs Nano 13 (2019) 9082-9090.
[12] Z.-W. Hu, M. Wang, C.-W. Guo, Z.-W. Shan, J. Li, W.-Z. Han, Graphene-coated tungsten nanowires deliver unprecedented modulus and strength, Materials Research Letters 7 (2019) 47-52.
[13] R. Ramachandramoorthy, W. Gao, R. Bernal, H. Espinosa, High Strain Rate Tensile Testing of Silver Nanowires: Rate-Dependent Brittle-to-Ductile Transition, Nano Letters 16 (2016) 255-263.
[14] H. Zheng, A. Cao, C.R. Weinberger, J.Y. Huang, K. Du, J. Wang, Y. Ma, Y. Xia, S.X. Mao, Discrete plasticity in sub-10-nm-sized gold crystals, Nature communications 1 (2010) 144.
[15] T. Zhu, J. Li, A. Samanta, A. Leach, K. Gall, Temperature and strain-rate dependence of surface dislocation nucleation, Physical Review Letters 100 (2008) 025502.

[16] H.S. Park, K. Gall, J.A. Zimmerman, Shape memory and pseudoelasticity in metal nanowires, Physical Review Letters 95 (2005) 255504.
[17] H.S. Park, K. Gall, J.A. Zimmerman, Deformation of FCC nanowires by twinning and slip, Journal of the Mechanics and Physics of Solids 54 (2006) 1862-1881.
[18] C.R. Weinberger, W. Cai, Plasticity of metal nanowires, Journal of Materials Chemistry 22 (2012) 3277-3292.
[19] Y. Yue, P. Liu, Q. Deng, E. Ma, Z. Zhang, X. Han, Quantitative evidence of crossover toward partial dislocation mediated plasticity in copper single crystalline nanowires, Nano letters 12 (2012) 4045-4049.
[20] B. Roos, B. Kapelle, G. Richter, C. Volkert, Surface dislocation nucleation controlled deformation of Au nanowires, Applied Physics Letters 105 (2014) 201908.
[21] S. Yin, G. Cheng, T.-H. Chang, G. Richter, Y. Zhu, H. Gao, Hydrogen embrittlement in metallic nanowires, Nature Communications 10 (2019) 2004.
[22] Y. Zhu, Mechanics of Crystalline Nanowires: An Experimental Perspective, Applied Mechanics Reviews 69 (2017) 010802.
[23] J.R. Greer, J.T.M. De Hosson, Plasticity in small-sized metallic systems: Intrinsic versus extrinsic size effect, Progress in Materials Science 56 (2011) 654-724.
[24] Y. Chen, X. An, X. Liao, Mechanical behaviors of nanowires, Applied Physics Reviews 4 (2017) 031104.
[25] S. Wang, Z. Shan, H. Huang, The Mechanical Properties of Nanowires, Adv. Sci. 4 (2017) 1600332.
[26] J.-H. Seo, Y. Yoo, N.-Y. Park, S.-W. Yoon, H. Lee, S. Han, S.-W. Lee, T.-Y. Seong, S.-C. Lee, K.-B. Lee, P.-R. Cha, H.S. Park, B. Kim, J.-P. Ahn, Superplastic Deformation of Defect-Free Au Nanowires via Coherent Twin Propagation, Nano Letters 11 (2011) 3499-3502.
[27] R.A. Bernal, A. Aghaei, S. Lee, S. Ryu, K. Sohn, J. Huang, W. Cai, H. Espinosa, Intrinsic Bauschinger Effect and Recoverable Plasticity in Pentatwinned Silver Nanowires Tested in Tension, Nano Letters 15 (2015) 139-146.
[28] Q. Qin, S. Yin, G. Cheng, X. Li, T.-H. Chang, G. Richter, Y. Zhu, H. Gao, Recoverable plasticity in penta-twinned metallic nanowires governed by dislocation nucleation and retraction, Nature communications 6 (2015) 5983.
[29] Y. Lu, J. Song, J.Y. Huang, J. Lou, Fracture of Sub-20nm Ultrathin Gold Nanowires, Advanced Functional Materials 21 (2011) 3982-3989.
[30] J. Wang, M. Tian, T.E. Mallouk, M.H. Chan, Microtwinning in template-synthesized single-crystal metal nanowires, The Journal of Physical Chemistry B 108 (2004) 841-845.
[31] C. Deng, F. Sansoz, Fundamental differences in the plasticity of periodically twinned nanowires in Au, Ag, Al, Cu, Pb and Ni, Acta Materialia 57 (2009) 6090-6101.
[32] T. Filleter, S. Ryu, K. Kang, J. Yin, R.A. Bernal, K. Sohn, S. Li, J. Huang, W. Cai, H.D. Espinosa, Nucleation-Controlled Distributed Plasticity in Penta-twinned Silver Nanowires, Small 8 (2012) 2986-2993.
[33] D. Jang, X. Li, H. Gao, J.R. Greer, Deformation mechanisms in nanotwinned metal nanopillars, Nature Nanotechnology 7 (2012) 594-601.
[34] Y. Zhu, Q. Qin, F. Xu, F. Fan, Y. Ding, T. Zhang, B.J. Wiley, Z.L. Wang, Size effects on elasticity, yielding, and fracture of silver nanowires: In situ experiments, Physical Review B 85 (2012) 045443.

[35] Z. Xie, J. Shin, J. Renner, A. Prakash, D.S. Gianola, E. Bitzek, Origins of strengthening and failure in twinned Au nanowires: Insights from in− situ experiments and atomistic simulations, Acta Materialia 187 (2020) 166-175.
[36] S. Narayanan, G. Cheng, Z. Zeng, Y. Zhu, T. Zhu, Strain hardening and size effect in five-fold twinned Ag nanowires, Nano letters 15 (2015) 4037-4044.
[37] Y.T. Zhu, X.L. Wu, X.Z. Liao, J. Narayan, L.J. Kecskés, S.N. Mathaudhu, Dislocation–twin interactions in nanocrystalline fcc metals, Acta Materialia 59 (2011) 812-821.
[38] S.H. Kim, H.K. Kim, J.H. Seo, D.M. Whang, J.P. Ahn, J.C. Lee, Deformation twinning of ultrahigh strength aluminum nanowire, Acta Materialia 160 (2018) 14-21.
[39] Z.X. Wu, Y.W. Zhang, D.J. Srolovitz, Dislocation–twin interaction mechanisms for ultrahigh strength and ductility in nanotwinned metals, Acta Materialia 57 (2009) 4508-4518.
[40] K. Lu, L. Lu, S. Suresh, Strengthening materials by engineering coherent internal boundaries at the nanoscale, Science 324 (2009) 349-352.
[41] Z.-H. Jin, P. Gumbsch, K. Albe, E. Ma, K. Lu, H. Gleiter, H. Hahn, Interactions between non-screw lattice dislocations and coherent twin boundaries in face-centered cubic metals, Acta Materialia 56 (2008) 1126-1135.
[42] Y. Zhu, X. Liao, X. Wu, Deformation twinning in nanocrystalline materials, Progress in Materials Science 57 (2012) 1-62.
[43] I.A. Ovid'ko, R.Z. Valiev, Y.T. Zhu, Review on superior strength and enhanced ductility of metallic nanomaterials, Progress in Materials Science 94 (2018) 462-540.
[44] X. Li, Y. Wei, L. Lu, K. Lu, H. Gao, Dislocation nucleation governed softening and maximum strength in nano-twinned metals, Nature 464 (2010) 877-880.
[45] Z. Cheng, H. Zhou, Q. Lu, H. Gao, L. Lu, Extra strengthening and work hardening in gradient nanotwinned metals, Science 362 (2018) eaau1925.
[46] X. Li, S. Yin, S.H. Oh, H. Gao, Hardening and toughening mechanisms in nanotwinned ceramics, Scripta Materialia 133 (2017) 105-112.
[47] Q. Huang, D. Yu, B. Xu, W. Hu, Y. Ma, Y. Wang, Z. Zhao, B. Wen, J. He, Z. Liu, Y. Tian, Nanotwinned diamond with unprecedented hardness and stability, Nature 510 (2014) 250-253.
[48] X. Liu, X. Chen, H.-A. Ma, X. Jia, J. Wu, T. Yu, Y. Wang, J. Guo, S. Petitgirard, C.R. Bina, Ultrahard stitching of nanotwinned diamond and cubic boron nitride in C2-BN composite, Scientific Reports 6 (2016) 30518.
[49] Y.A. Shin, S. Yin, X. Li, S. Lee, S. Moon, J. Jeong, M. Kwon, S.J. Yoo, Y.-M. Kim, T. Zhang, H. Gao, S.H. Oh, Nanotwin-governed toughening mechanism in hierarchically structured biological materials, Nature Communications 7 (2016) 10772.
[50] N. Malyar, J.-S. Micha, G. Dehm, C. Kirchlechner, Dislocation-twin boundary interaction in small scale Cu bi-crystals loaded in different crystallographic directions, Acta Materialia 129 (2017) 91-97.
[51] L. Zhong, F. Sansoz, Y. He, C. Wang, Z. Zhang, S.X. Mao, Slip-activated surface creep with room-temperature super-elongation in metallic nanocrystals, Nature Materials 16 (2017) 439-445.
[52] G.M. Cheng, C.Y. Miao, Q.Q. Qin, J. Li, F. Xu, H. Haftbaradaran, E.C. Dickey, H.J. Gao, Y. Zhu, Large anelasticity and associated energy dissipation in single-crystalline nanowires, Nature Nanotechnology 10 (2015) 687-691.

[53] C.-N. Jennifer, Y. Dachi, K. Jae-Woo, P. Cheol, F.F. Luis, Mechanical characterization of pristine and hydrogen-exposed palladium nanowires by in situ TEM, Nanotechnology 24 (2013) 035701.
[54] G. Cheng, Y. Zhang, T.-H. Chang, Q. Liu, L. Chen, W.D. Lu, T. Zhu, Y. Zhu, In situ nano-thermo-mechanical experiment reveals brittle to ductile transition in silicon nanowires, Nano Letters 19 (2019) 5327-5334.
[55] W. Tao, P. Cao, H.S. Park, Atomistic simulation of the rate-dependent ductile-to-brittle failure transition in bicrystalline metal nanowires, Nano letters 18 (2018) 1296-1304.
[56] B. Wiley, Y. Sun, Y. Xia, Synthesis of silver nanostructures with controlled shapes and properties, Acc Chem Res 40 (2007) 1067-1076.
[57] Y. Zhu, N. Moldovan, H.D. Espinosa, A microelectromechanical load sensor for in situ electron and x-ray microscopy tensile testing of nanostructures, Applied physics letters 86 (2005) 013506.
[58] G. Cheng, S. Yao, X. Sang, B. Hao, D. Zhang, Y.K. Yap, Y. Zhu, Evolution of Irradiation-Induced Vacancy Defects in Boron Nitride Nanotubes, Small 12 (2016) 818-824.
[59] S. Plimpton, Fast Parallel Algorithms for Short-Range Molecular-Dynamics, J Comput Phys 117 (1995) 1-19.
[60] P. Williams, Y. Mishin, J. Hamilton, An embedded-atom potential for the Cu–Ag system, Modelling and Simulation in Materials Science and Engineering 14 (2006) 817.
[61] Y. Zhu, H.D. Espinosa, An electromechanical material testing system for in situ electron microscopy and applications, Proceedings of the National Academy of Sciences of the United States of America 102 (2005) 14503-14508.
[62] T.H. Chang, G.M. Cheng, C.J. Li, Y. Zhu, On the size-dependent elasticity of penta-twinned silver nanowires, Extreme Mechanics Letters 8 (2016) 177-183.
[63] C. Li, D. Zhang, G. Cheng, Y. Zhu, Microelectromechanical Systems for Nanomechanical Testing: Electrostatic Actuation and Capacitive Sensing for High-Strain-Rate Testing, Experimental Mechanics 60 (2020) 329-343.
[64] C. Deng, F. Sansoz, Repulsive force of twin boundary on curved dislocations and its role on the yielding of twinned nanowires, Scripta Materialia 63 (2010) 50-53.
[65] E. Ma, T. Zhu, Towards strength–ductility synergy through the design of heterogeneous nanostructures in metals, Materials Today 20 (2017) 323-331.
[66] X. Liu, F. Yuan, Y. Zhu, X. Wu, Extraordinary Bauschinger effect in gradient structured copper, Scripta Materialia 150 (2018) 57-60.
[67] J. Rajagopalan, J.H. Han, M.T.A. Saif, Plastic deformation recovery in freestanding nanocrystalline aluminum and gold thin films, Science 315 (2007) 1831-1834.
[68] K.M. Davoudi, L. Nicola, J.J. Vlassak, Bauschinger effect in thin metal films: Discrete dislocation dynamics study, Journal of Applied Physics 115 (2014) 013507.